PHYSICAL REVIEW B **00**, 005100 (2016)

Core-level attosecond transient absorption spectroscopy of laser-dressed solid films of Si and Zr

Enikoe Seres,[1,*] Jozsef Seres,[1] Carles Serrat,[2] and Shinichi Namba[3]
[1]*Institute of Atomic and Subatomic Physics - E141, Vienna University of Technology, Stadionallee 2, 1020 Vienna, Austria*
[2]*Universitat Politècnica de Catalunya, Departament de Física, Colom 11, 08222 Terrassa, Spain*
[3]*Graduate School of Engineering, Hiroshima University, 1-4-1 Kagamiyama, Higashi-Hiroshima, Hiroshima 739-8527, Japan*
(Received 15 June 2016; revised manuscript received 22 August 2016; published xxxxxx)

We investigated experimentally as well as theoretically the ultrafast response of the wave function of the conduction band (CB) of Si and Zr to a near-infrared laser field using extreme ultraviolet (XUV) absorption spectroscopy in the spectral range of 80–220 eV. The measured dynamics of the XUV transmission demonstrates that the wave function of the CB follows the electric field of the dressing laser pulse. In these terms, laser dressing was earlier mainly studied on gases. Measurements with two-femtosecond and 200-attosecond temporal steps were performed in the vicinity of the Si $L_{2,3}$ edge near 100 eV, the Si L_1 edge near 150 eV, and the Zr $M_{4,5}$ edge near 180 eV. The observed changes were dependent on the core states being excited by the XUV probe pulse. At the $2p$ to CB transitions of Si, the XUV transmission increased via the effect of the dressing laser pulse, while at the $2s$ to CB transition of Si and the $3d$ to CB transition of Zr, the XUV transmission decreased. Furthermore, beats between the transition from $2p_{1/2}$ and $2p_{3/2}$ levels of Si and from $3d_{3/2}$ and $3d_{5/2}$ levels of Zr were observed with 20.7 fs and 3.6 fs periods.

DOI: 10.1103/PhysRevB.00.005100

I. INTRODUCTION

Time resolved x-ray absorption spectroscopy (XAS) and transient absorption spectroscopy has an old tradition and modern importance. Authentic experiments with highest and highest resolution guide us within the sometimes ambiguous maze of the theoretical predictions. With experimental support, a deeper understanding of the electronic properties of materials and the underlying processes of light-matter interactions can be gained to develop faster electronics and optical detectors even up to PHz frequencies [1], with also a strong binding to chemical physics and chemistry.

The spectroscopy of laser-dressed materials is a unique branch within x-ray spectroscopy. It measures the response of the electronic system of materials to the field of the pump laser itself [2] without electron excitation and subsequent absorption of the pump. Consequently, it provides information about the processes within an optical period of the laser pulse with femtosecond and subfemtosecond temporal resolution [3]. Theoretically, it is described as the manipulation of the electron-wave-packet dynamics of the unoccupied and occupied electronic states of the material [4].

For atomic and molecular gases such as argon [5], neon [6], helium [7,8], N_2 [9], Br_2 [10], and hydrocarbons [11], many brilliant experimental testimonial results occur. They probed mainly valence electrons and exited them to levels near the ionization threshold with extreme ultraviolet (XUV) probe in the range of 10, 20 eVs. Core-level excitation as probe [3,12–14] were the subject of fewer studies. Besides the change in absorption, Stark shift in He [15] and Ar [5], Rabi oscillations [16] in Ne, line broadening [5], and quantum beats [17,18] were recognized in the recorded XUV or photoelectron spectra.

Besides the basic processes and interactions in atoms and molecules, understanding multiparticle correlation and associated phenomena in solids is a key factor in material science. In our paper, we demonstrate the laser field dressing of solid Si and Zr thin films and examine them with core-level transient absorption spectroscopy. Time resolved spectroscopy of Si L-edge near 100 eV was the subject of pioneering studies, reaching nanosecond [19] and later picosecond [20] temporal resolution. As short as 20 fs temporal resolution was achieved at the L-edge [21,22] and at the K-edge (near 1.8 keV) in Si, [23,24] and laser-excited phonons, and the dynamics of interband electron excitations were measured. Attosecond-scale temporal resolution was demonstrated in SiO_2 dielectrics [25], where the application of the suitably high laser intensity beyond the critical field strength injected electrons into the conduction band (CB). In other experiments, interband electron excitation dynamics was resolved in subcycle resolution in Si [26] in a wide bandgap semiconductor of GaN [27], and photo-induced charge transfer was examined in Co_3O_4 [28] with transient XUV spectroscopy. In spite of these achievements, the yet unexplored phenomena in molecules and solids offer abundant challenges for scientists.

In the present paper, we examine thin Si and Zr films dressed by the near-infrared (NIR) pulses of a Ti:sapphire laser system. Contrary to earlier studies, which were focused on understanding electron excitation [25–27] or charge migration [28], our aim is to observe the effect of the laser electric field on the CB. For detecting the changes on the CB wave function, the delay dependence of the XUV transmission from different core levels to the CB is measured, namely, the $2p$ and $2s$ to CB transitions of Si in the vicinity of 100 eV and 150 eV, respectively, and the $3d$ to CB transitions of Zr in the vicinity of 180 eV. Both the slow change in transmission caused by the envelope of the dressing laser pulse, the fast change due to its electric field carrier, and the quantum beats with 20.7 fs and 3.6 fs periods between the transitions from $2p_{1/2}$ and $2p_{3/2}$ levels of Si and from $3d_{3/2}$ and $3d_{5/2}$ levels of Zr are studied. Furthermore, we demonstrate that the above-mentioned changes in the XUV transmission caused by the laser dressing can be distinguished from the

*enikoe-judit-seres@lycos.com

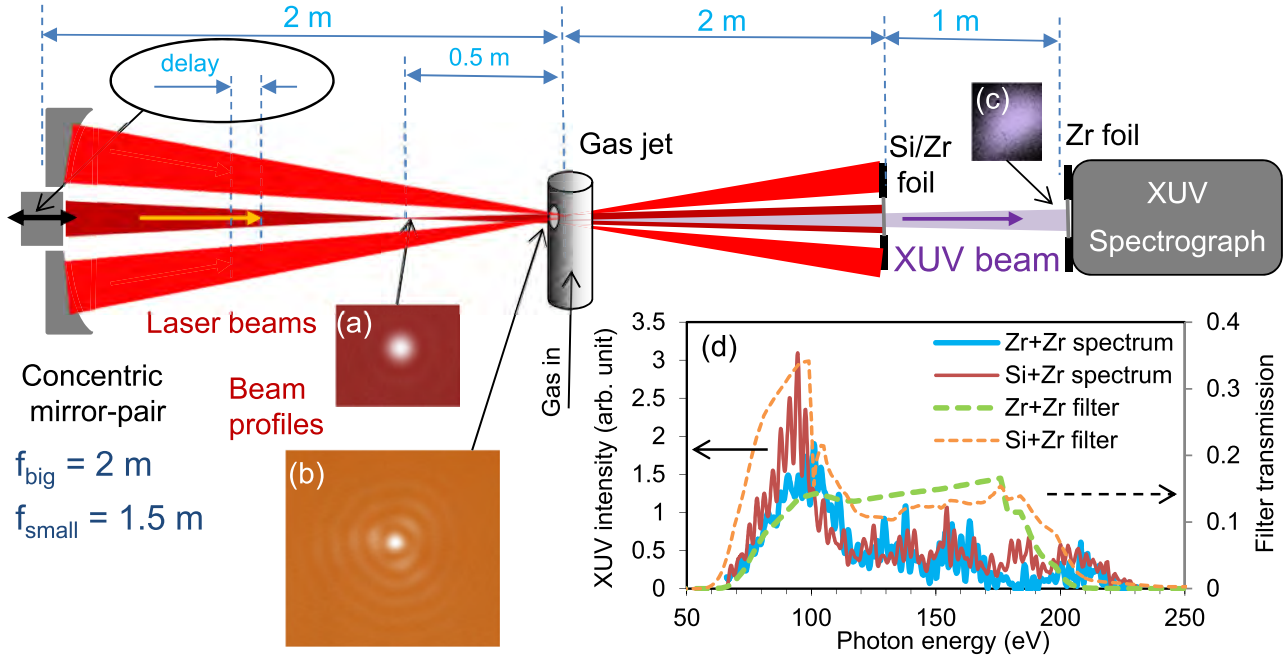

FIG. 1. Experimental setup. A concentric mirror pair was used for pump-probe spectroscopy. The inner mirror was movable for adjustable delay and served as the NIR pump. In the focus of the outer mirror [beam profile of inset (b)], high harmonics were generated [beam profile of inset (c)] for XUV probe with spectra [inset (d)] after two sets of thin foils of Zr+Zr or Si+Zr, as indicated.

ones caused by the generated optical phonons and electronic excitations.

II. EXPERIMENTAL SETUP

The laser pulses of a Ti:sapphire laser system (pulse duration: 35 fs ; central wavelength: 805 nm; repetition rate: 10 Hz) were loosely focused with a concentric mirror pair (see Fig. 1). The inner mirror (having a focal length of 1500 mm) focused the 7 mJ/pulse part of the laser beam at 500 mm before a gas jet. The gas jet was made from a metal tube with diameter of 3 mm. A hole with diameter of 1 mm was drilled perpendicular through the tube, and the tube was placed perpendicular to the laser beam (see Fig. 1). One end of the tube was closed, and from the other side, it was filled with Ne gas with adjustable pressure. Some part of the central laser beam passed through the 1 mm diameter hole in the jet and was illuminated with a 5 mm diameter surface of the examined foils of 50-nm-thick Si or 200-nm-thick Zr with a peak intensity of $\sim 1.5 \times 10^{11}$ W/cm^2 ($\sim$1 V/nm). This served as pump or dressing and altered the electronic configuration of the thin foil (see Fig. 1). The outer mirror, having a focal length of 2000 mm, focused the beam into the gas jet, which served as high harmonic source to produce the trains of $\sim$200 attosecond pulses for the probe [29,30]. The optimal laser intensity for the source was adjusted with a motorized aperture. The outer mirror produced a ring structure distribution at the focus with a well distinguishable intense central beam part. This central beam part had a diameter of 110 μm and contained a $\sim$8 mJ/pulse part of the laser beam, giving a peak intensity of $\sim 1.5 \times 10^{15}$ W/cm^2, expecting the Gaussian pulse shape. A 300-nm-thick Zr foil was used between the XUV spectrometer and the HHG source chamber, with the purpose of separating the vacuum and adequately blocking the laser beam and the low energy part of the XUV beam. While the calculated cutoff energy of the harmonics was $\sim$300 eV, the measured spectra extended to about 230 eV, as can be seen in the inset of Fig. 1(d), and it was limited also by the transmission of the Zr foil. The beam profiles of the laser beams in the focus of the mirrors and the ones of the harmonic XUV beam at the entrance of the XUV spectrometer were measured and are plotted in the insets of Figs. 1(a)–1(c), respectively. Two measured XUV spectra are also shown in the inset of Fig. 1(d), which correspond to the two different filters inserted into the XUV beam in the case of a Ne backing pressure of 1.6 bars. The blue line is the spectrum with the Zr foil (Zr+Zr) and the red one with the Si foil (Si+Zr). The measured XUV spectra extend from $\sim$70 eV to $\sim$230 eV. Also in the inset of Fig. 1(d), one can observe that the transmitted XUV spectrum after the Si foil was stronger before the Si L-edge (100 eV) and after the Zr M-edge (180 eV), as can be expected from the calculated transmission curves of the foil combinations. The concentric mirror pair ensured the accurate delay between the probe and pump pulses, which was changed by moving the inner mirror with 0.2 fs accuracy.

III. EXPERIMENTAL RESULTS

A. Studied process

In this paper, we examine thin solid foils by XAS. For the pump-probe experiment, thin Si and Zr foils were chosen because they have suitable absorption edges within the generated XUV probe spectral range of 70 eV to 230 eV [Fig. 1(d)], namely the Si $L_{2,3}$ edge at $\sim$100 eV, the Si L_1 edge at $\sim$150 eV [31,32], and the Zr $M_{4,5}$ edge at $\sim$180 eV [32]. We were hence able to study electron transitions from the $2p$,

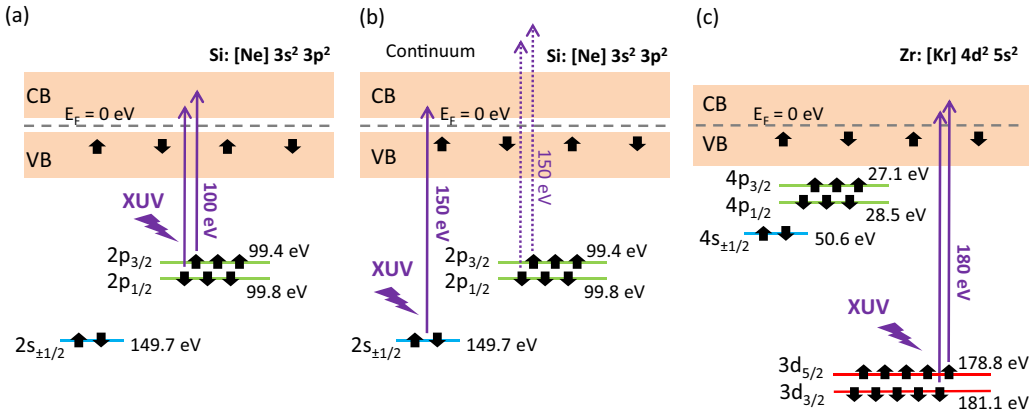

FIG. 2. Electron transitions were examined from the (a) $2p$, (b) $2s$, and (c) $3d$ core levels of Si and Zr to the conduction band (CB) near 100 eV, 150 eV, and 180 eV, respectively.

$2s$, and $3d$ core levels to the CB of Si and Zr, as presented in Fig. 2.

The foils were illuminated with short x-ray pulses in the XUV spectral range with energy suitable to move a core electron to an unoccupied level of the CB, as presented in Fig. 3. The transmitted XUV signal can be written in the usual form $T = e^{-\sigma_a n_a d}$, where T is the transmission, σ_a is the absorption cross-section of the material at the XUV wavelength, n_a is the atomic density, and d is the thickness of the material. The solid film was also illuminated by NIR laser pulses from a Ti:sapphire laser. The field of the NIR laser pulses modified the transmission of the XUV beam by altering the absorption cross-section. The resulting small change in the transmission can be expressed as

$$\Delta T \approx \left.\frac{\partial T}{\partial \sigma_a}\right|_0 \Delta\sigma_a = -T_0 n_a d\,\Delta\sigma_a, \qquad (1)$$

with T_0 being the field-free transmission. In our time resolved experiment, the change of the transmission $\Delta T(\tau)$ via the delay (τ) between the NIR and XUV pulses was measured. This change can be understood theoretically by means of the change in the absorption cross-section $\Delta\sigma_a(\tau)$. The laser field polarized the material, which means that the laser field modified the originally symmetric periodic potential (thin gray line in Fig. 3) to an asymmetric one (thin dashed red line). Consequently, the wave function of the electronic level in the CB (thick gray line) was appropriately modified (thick dashed red line). Because σ_a depends on the wave functions of the core and CB levels, a change of the transmission can be obtained [see Eq. (A18)] in the Appendix for a detailed description):

$$\Delta T_j \approx \pm T_j I_0(\tau)\sin^2(\omega_0\tau)\cos^4(\Omega\tau). \qquad (2)$$

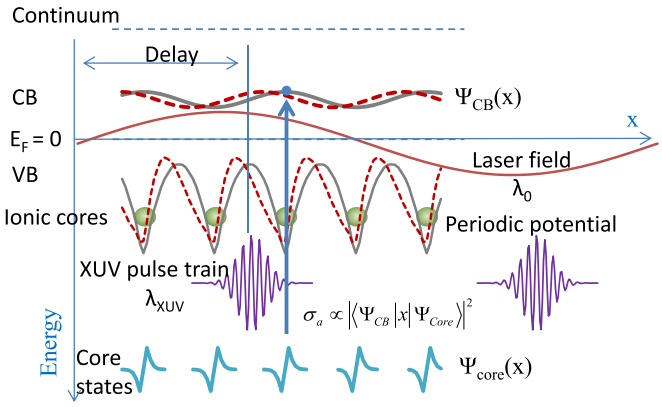

FIG. 3. Visualization of the core electron excitation within a laser-dressed solid. The laser field modifies the periodic potential and the wave function of the CB from the original (gray solid lines) to the dressed (dashed red lines). Consequently, the probability of the XUV pulse induced core → CB transition changes. Note that the scaling of the laser field and the XUV field was modified for a better visibility because even the wavelength of the XUV field is much larger than the distance between the atoms.

In Eq. (2), the index $j = 2p, 2s$, or $3d$ represents the core electron levels involved in the electron excitation (see Fig. 2). The sign (+) corresponds to the $2p \rightarrow$ CB transition and the sign (−) is valid for the $2s \rightarrow$ CB and the $3d \rightarrow$ CB transitions. $T_j = T_{j,m=\mathrm{CB}}$ is a constant that depends on the material and the involved transitions as it is defined in the Appendix.

As seen in Eq. (2), the XUV transmission is expected to be modified by three different effects, namely, (i) by a slow change via the $I_0(\tau)$ envelope of the laser pulse; (ii) by a fast modulation defined by the central angular frequency ω_0 of the laser field; and (iii) by a beat signal between two alternative absorption paths with $\Omega = \Delta E/2\hbar$, where ΔE is the energy difference between the sublevels of the core electronic levels ($2p_{3/2}$ and $2p_{1/2}$ or $3d_{5/2}$ and $3d_{3/2}$), as shown in Fig. 2. A beat signal cannot be expected at the transition from the $2s$ level because it contains no sublevels (i.e., $\Omega = 0$). The 805 nm wavelength of the laser produces a fast oscillation in the transmitted XUV signal with a frequency of 745.3 THz or a period of 1.34 fs. In the case of Si, the energy difference between the $2p_{1/2}$ and $2p_{3/2}$ levels [32] is 0.4 eV, meaning a beat frequency of 48.4 THz or a period of 20.7 fs. For the $3d_{3/2}$ and $3d_{5/2}$ levels [32] of Zr, these values are 2.3 eV, 278.0 THz, and 3.6 fs , respectively. While the pulse envelope of 35 fs and the 20.7 fs beat in Si can be resolved with a temporal resolution of a few femtoseconds, the fast 1.34 fs oscillation caused by the laser field and the 3.6 fs beat in the Zr can be measured only with attosecond (sub-fs) temporal resolution.

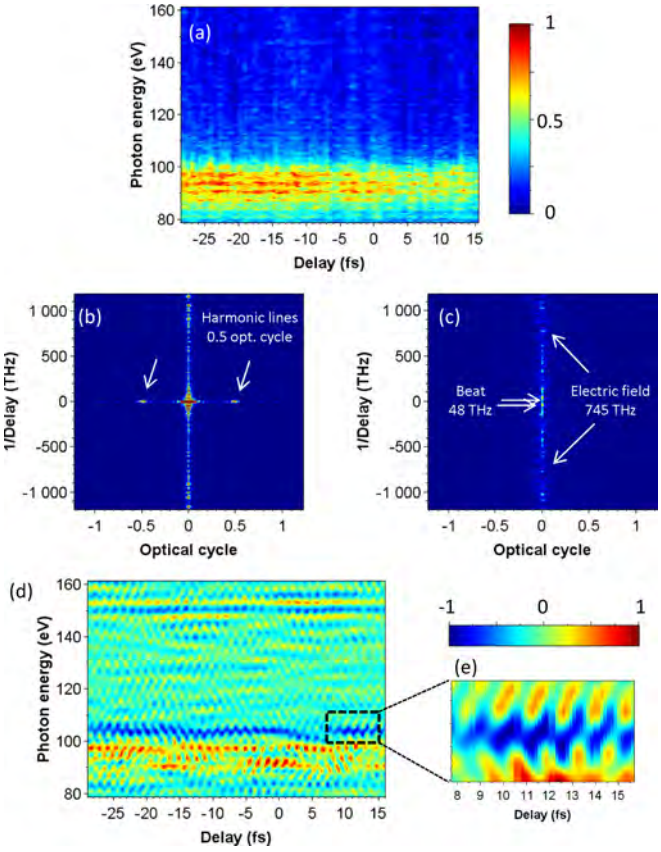

FIG. 4. Method of data evaluation. (a) Spectra series were measured as a function of delay between the NIR pump and XUV probe pulses. (b) The 2D Fourier transform of (a). (c) The 2D Fourier transform of (a) with dc subtraction. (d) Inverse Fourier transformed spectra series after filtering. (e) The highlighted part of (d) was magnified to present the competition between the core → CB and core → VB transitions, which altered the induced absorption to induced transmission within 0.67 fs and vice versa. The color scales are normalized, and direction from blue to red means an increase of transmitted XUV signal. See details in text.

B. Data evaluation

During the measurements, the transmitted XUV spectra were recorded within the 70–230 eV spectral range with 2 fs or 0.2 fs delay steps. The spectrograph and detector had a spectral resolution of ∼0.015 nm, which meant ∼0.1 eV and ∼0.4 eV resolution at around 100 eV and 180 eV, respectively. To examine how the measurement data were evaluated, we present here an example of a measurement that was performed with 0.2 fs delay steps and where Si was examined. A set of transmitted XUV spectra within a measurement series is plotted in Fig. 4(a). A measurement series contains the effect of several physical processes, which were hardly recognizable together. One immediately can see that the transmitted XUV signal decreased below 100 eV during the time the laser illuminated the foil, which should have been the consequence of interband electron excitation. This change dominated over others. Furthermore, the generated harmonics were most intense near 100 eV, and the change near 150 eV is hardly visible. To recognize and distinguish smaller effects both in the spectrum and in time and suppress noise, we further evaluated the measurement to highlight data channels of interest and suppress others. Therefore, the measured two-dimensional (2D) data set was Fourier transformed [see Fig. 4(b)]. The horizontal axis is the transform along the photon energy measured in harmonic orders and gives the scale in optical cycles. The vertical axis is the transform along the delay. The contribution of the harmonic lines is recognizable by the peak at 0.5 optical cycles, and this transform is usable to make appropriate filtering in the spectral direction. In the direction of the delay, a small change sits on a large dc level. To avoid artifacts, another 2D Fourier transform was calculated after subtracting the dc level [see Fig. 4(c)]. On this transform, the peaks of the effect of the laser electric field at 754 THz and the peaks of the beat at 48 THz can be recognized. This transform was used for filtering in the direction of delay. Using appropriate Fourier filters, which are presented in the next sections, the measurement results take the form of Fig. 4(d). In the figure, beyond the $2p \rightarrow$ CB transition near 100 eV, the effect of the pump to the $2s \rightarrow$ CB transition near 150 eV became also well visible. The effect of the beat with the 21 fs period can be recognized near 100 eV. The fast effect of the laser electric field with a 1.34 fs period also appears with high contrast near 100 eV and 150 eV, while in the range between 110 eV and 140 eV the colors are smooth; some periodicity is visible only as noise with low contrast, as can be expected. A small part in the range of the Si L-edge is magnified and put to Fig. 4(e). The oscillation between the $2p \rightarrow$ CB and $2p \rightarrow$ valence band (VB) transitions at the effect of the laser field can be well observed as the laser field induced additional absorption or transmission and switched between the two absorption channels within a time of 0.67 fs.

C. Measurements with femtosecond resolution

Pump-probe measurement series were performed for Si and Zr foils. The transmitted XUV spectra at a set of delays were measured and evaluated around 100 eV, 150 eV, and 180 eV to study the $2p$, $2s$, and $3d$ to CB transitions, respectively. The delay between the dressing laser pulse and the probe XUV pulse train was scanned with 2 fs temporal resolution. It is clear from Eqs. (A10) and (A11) of the Appendix that without a laser pump ($\alpha_1 = 0$), one can expect strong absorption at the $2p \rightarrow$ CB transition and weak absorption at the $2s \rightarrow$ CB and $3d \rightarrow$ CB transitions. This is the straight consequence of the symmetry of the wave functions, namely that the wave function of $2p$ is antisymmetric while those of $2s$, $3d$, and CB are symmetric.

To follow the effect of the dressing laser, 2D Fourier transforms of the measured spectra series were calculated and are plotted in Figs. 5(e) and 5(f) for the direction corresponding to the delay axis. In the case of Si, two subsequent measurement series were recorded in different delay intervals, and the calculated Fourier transforms are plotted with solid and dashed blue lines in Fig. 5(e). These transforms contain the well distinguishable peak at ∼48 THz, which belong to the beat between $2p_{3/2}$ and $2p_{1/2}$ levels. The appearance of the peak at ∼14 THz (∼70 fs) should be the LO phonon in Si [33]. In the Fourier transform of the Zr measurement [Fig. 5(f)], one can recognize low frequency peaks at ∼5 THz, ∼12 THz, and ∼20 THz, which are probably

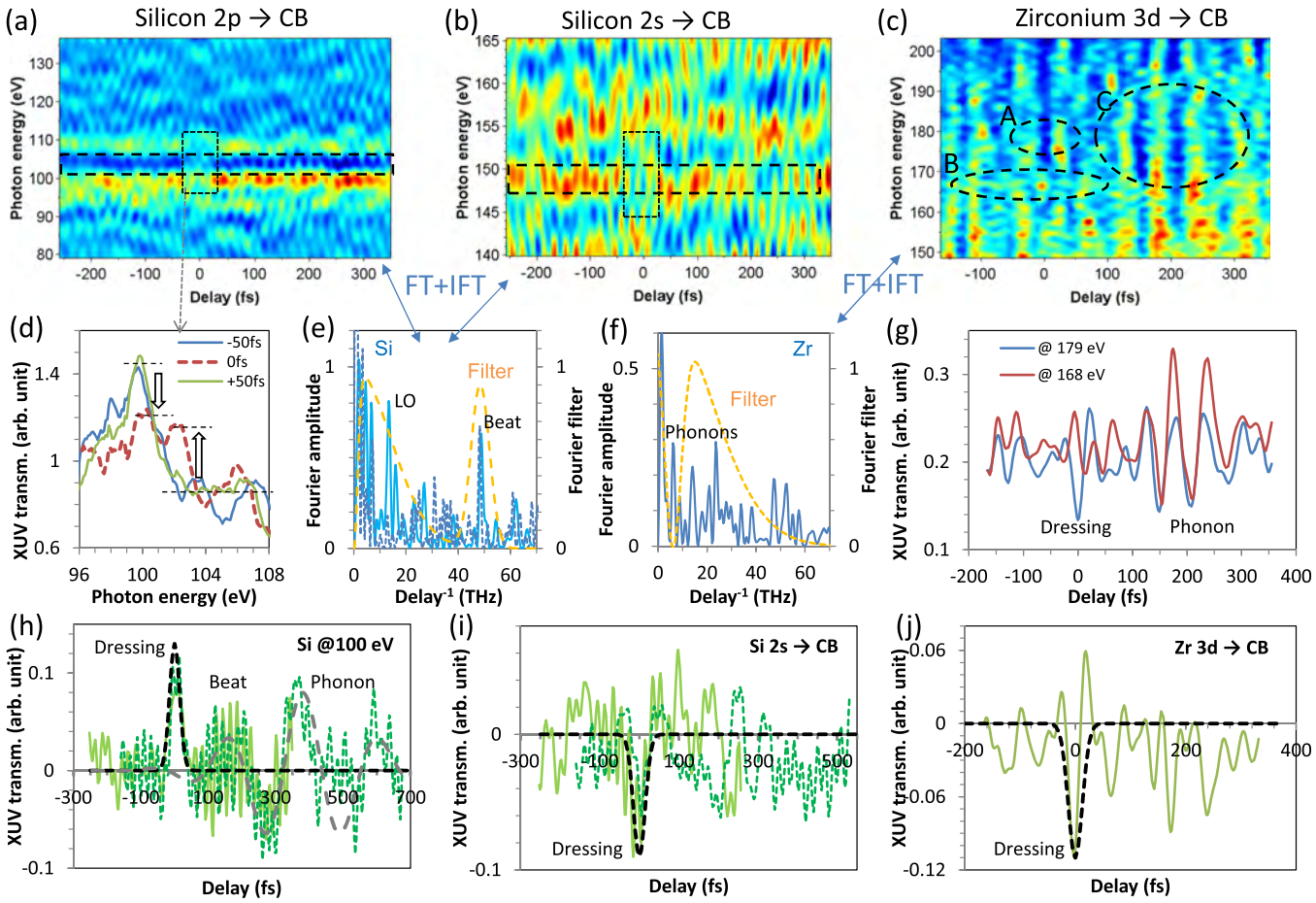

FIG. 5. The XUV transmission spectra were measured and evaluated at around (a) Si $L_{2,3}$, (b) Si L_1, and (c) Zr $M_{4,5}$ edges with femtosecond temporal resolution. (d) The transmitted XUV signal was essentially altered in the presence of the pump NIR laser pulse (red dashed line), e.g., at the $L_{2,3}$ edge of Si. (e), (f) The 2D Fourier transforms of the measured data sets were used to identify involving processes, and suitable Fourier filters were applied to evaluate the measurements and to produce panels (a)–(c). (g)–(j) The evaluated results are plotted together with the theoretical predictions (see details in the text). While (d) and (g) plot the XUV transmission itself, (h)–(j) are the change of the transmission. The normalized color scales are the same as in Fig. 4(e).

produced by phonon modes in the bulk Zr or in the oxidized surface layer [34]. The beat between the $3d_{5/2}$ and $3d_{3/2}$ levels of Zr (278 THz, 3.6 fs) is too fast to be observed with the 2 fs temporal resolution; therefore, we analyze it using higher temporal resolution in Sec. II.D. In order to highlight the processes of interest, to suppress the high frequency noise, to eliminate the 5 THz phonon in Fig. 5(f), and for a better visibility, appropriate Fourier filters [orange dashed lines in Figs. 5(e) and 5(f)] were applied. The filtered spectra series are plotted in Figs. 5(a)–5(c), and the interesting parts are highlighted with black dashed frames.

The time resolved change of the transmission at the examined $L_{2,3}$, L_1, and $M_{4,5}$ edges are separately plotted in Figs. 5(h)–5(j) by calculating the difference between the signal at the edges and the background far from the edges. One can see on this figure that when the laser pulse arrives (near zero delays), the transmission increases after the $L_{2,3}$ edge and decreases at the L_1 and $M_{4,5}$ edges. At small delays [black thin dashed frame in Fig. 5(a)], the $L_{2,3}$ edge almost disappears. To highlight this range, unfiltered raw spectral data at three different delays are plotted in Fig. 5(d). While at the delays of ± 50 fs , the edge is well visible and undisturbed; at 0 fs delay (red dashed line), the transmission is increased just after the edge and decreases just before the edge to almost the same transmission value.

The delay dependence of the transmitted XUV signals through the Si foil is plotted in Figs. 5(h) and 5(i) at 101 eV for the $2p \rightarrow$ CB transition and at 147 eV for the $2s \rightarrow$ CB transition, respectively, considering two subsequent measurement series in different delay ranges (solid and dashed green lines). At around zero delays, the transmission follows the envelope of the laser pulse (black dashes line), as expected from the theory, namely an increase for the $2p \rightarrow$ CB and a decrease for $2s \rightarrow$ CB transitions were observed. At positive delays in Fig. 5(h), the transmitted signal is clearly modulated by the beat (~21 fs) between the $2p_{3/2}$ and $2p_{1/2}$ levels. In Fig. 5(i), there is no beat, as expected in the case of the $2s \rightarrow$ CB transition [some residual beat can be observed from the $2p$ to continuum transitions, though, as noted in Fig. 2(b)]. The beat in Fig. 5(h) relaxes at ~300 fs delay. For higher delays, the laser pulse produces a long-period ~200 fs modulation (gray dashed line), which can probably be associated to the TO phonon. This effect cannot be clearly identified because of the short measurement time <700 fs.

The surface plot shown in Fig. 5(c) for the Zr measurement shows several features. At photon energies in the range of 180 eV and at negative delays, the colors are mainly light blue and yellow, meaning low absorption (high transmission). At near zero delays (frame A), it turns to dark blue, meaning high absorption. Still around 180 eV and at higher positive delays, it becomes again light blue–yellow, and it starts to change and oscillate at higher delays, especially in the delay range of 100–300 fs (frame C). We associate this oscillation to the generated ∼20 THz phonons [35]. At lower photon energies near 165–170 eV (out of the range of the CB) and below 100 fs delay (frame B), the colors in the surface plot remain light blue and yellow; this means an almost delay-independent transmission, and the change by the phonons appears only between the 100–300 fs delay range. This means that the effect of laser dressing is observed at near-zero delays and at certain spectral range, which is different from the phonon assisted oscillations (e.g., frame C) observed at positive delays and almost independently of the XUV energy.

The just mentioned processes observed from Fig. 5(c) for the Zr measurement are further detailed in the curves shown in Fig. 5(g). The XUV transmission at 179 eV (blue line) shows a well distinguishable minimum at zero delay during the laser pulse due to laser dressing and a strong oscillation between 100 and 300 fs due to phonons. Far below the edge at around 168 eV (red line), only the strong oscillation between 100 and 300 fs due to phonons can be seen. In the difference [Fig. 5(j)] of the signal (179 eV) and the background (168 eV), the appearance of the strong absorption at zero delay due to laser dressing can be well observed, while the effect of the phonons mainly disappears because they are there in both spectral ranges.

D. Measurement with attosecond resolution

Our measurement series of Sec. II.C were repeated at around zero delay, with a much higher 0.2 fs temporal resolution in order to study in more detail the effect of the dressing of the laser pulse on the thin Si and Zr foils. Aiming at studying the beating and the effects of the electric field dressing in the spectral ranges of the three interested transitions, the measured data sets were processed to produce Figs. 6(a)–6(c) by applying appropriate Fourier filters [Figs. 6(d)–6(f)].

For both Si and Zr, the Fourier transforms along the delay axis contain a peak at ∼745 THz, which belongs to the electric field square of the laser beam. It is especially well distinguishable in Fig. 6(f) (Zr measurement). In the case of Zr, another peak at 278 THz (3.6 fs , 2.3 eV), which belongs to the beat between the $3d_{5/2}$ and $3d_{3/2}$ core states (CSs), is well visible. The 48 THz beat between $2p_{3/2}$ and $2p_{1/2}$ levels of Si is not observable in Fig. 6(e) because of the inadequate resolution; however, it is well visible in Figs. 6(a) and 6(b), and the similarities with the theoretical calculation for He [Fig. 3(a) in Ref. [18] can be immediately recognized. The origin of the peak appearing at 180–200 THz in Fig. 6(f) is unclear, and, hence, we filtered it out.

The presence of the harmonic lines and the shape of the spectrum at around 100 eV can essentially diminish the visibility of the signal of our interest. Therefore, for the evaluation of the measurement results of Si, the spectral effect of the harmonic lines [peak at 0.5 optical cycles in Fig. 6(d) (red lines)] and the slow and fast components of the spectra were filtered out (orange dashed line). Contrary to Si, of which direct band transition starts at ∼3.4 eV and, consequently, absorbs the 805 nm laser light weakly, Zr is a metal and absorbs the laser light strongly. This means strong band-to-band electron excitation and, consequently, a much stronger effect of the illuminating laser pulse to the XUV transmission due to excited electrons. With the intention to observe this effect also, and because harmonic lines cannot be resolved at such high photon energies, we did not filter out the slow spectral components and harmonic lines in the evaluation of the Zr measurement data [blue dashed line in Fig. 6(d)] as we did for Si. Otherwise, the 180 eV edge of the Zr is in the HHG plateau; therefore, the spectral shape of the HHG does not affect the visibility of the signal.

In both the Si and Zr, the measured XUV spectra were recorded with 200 as delay steps in two subsequent measurement series with different, partly overlapping delay ranges. The surface plots in Figs. 6(a)–6(c) show only the first series, but both series are plotted in Figs. 6(d)–6(j) with dashed and solid lines. In the surface plots of Figs. 6(a) and 6(b), the effect of the delay scan is well visible at around the $L_{2,3}$ and L_1 edges of Si at 100 eV and 150 eV, respectively, which is marked with black dashed frames. The delay dependence of the XUV transmission at 102 eV (±1 eV range) and at 150 eV (±2 eV range) is averaged and plotted in Figs. 6(h) and 6(i). On the surface plot of Fig. 6(c) corresponding to the Zr measurement, the dressing effect of the laser is hardly seen because, as mentioned earlier, the change of the transmission is dominated by the laser-excited electrons between the VB and the CB. The transmitted XUV signals [evaluated from the two marked areas in Fig. 6(c)] continuously increase with the delay [see Fig. 6(g), where the two curves are shifted for a better visibility], and they follow the main trend of the integrated Gaussian laser pulse (dashed black line) and decay after the laser pulse. The calculated difference of the signal (180 eV) and the background (160 eV) is potted in Fig. 6(j).

The high frequency modulation, which can be seen in every evaluated delay curve in Figs. 6(h)–6(j), is the consequence of the square of the electric field (carrier) of the laser pulse. The slow changes of the XUV transmission are due to the envelope of the pulse (black dashed lines). In Figs. 6(k)–6(m), the calculated signals are presented according to the theory. For the calculation, we used the modified form of Eq. (2),

$$\Delta T_j \approx \pm\tfrac{1}{8} T_j I_0(\tau)[1 - V_0 \cos(2\omega_0\tau)][1 + V_b \cos(2\Omega\tau)]^2, \tag{3}$$

and assumed that it is not possible to make a measurement with full visibility of the fast oscillation V_0 and the beat V_b because of the limited temporal resolution and may not fully be the equidistance train of XUV attosecond pulses. The comparison with the measured curves gave us visibility values of 0.6 and −0.15, respectively. Comparing the measured curves with the calculated ones, a very good agreement can be observed. The measurement results exhibit every theoretically expected process, namely the transmission change with the laser pulse envelope, the fast oscillation with the doubled laser central frequency, and the ∼21 fs and ∼3.6 fs beat for Si and Zr, respectively. Some additional temporal structure within

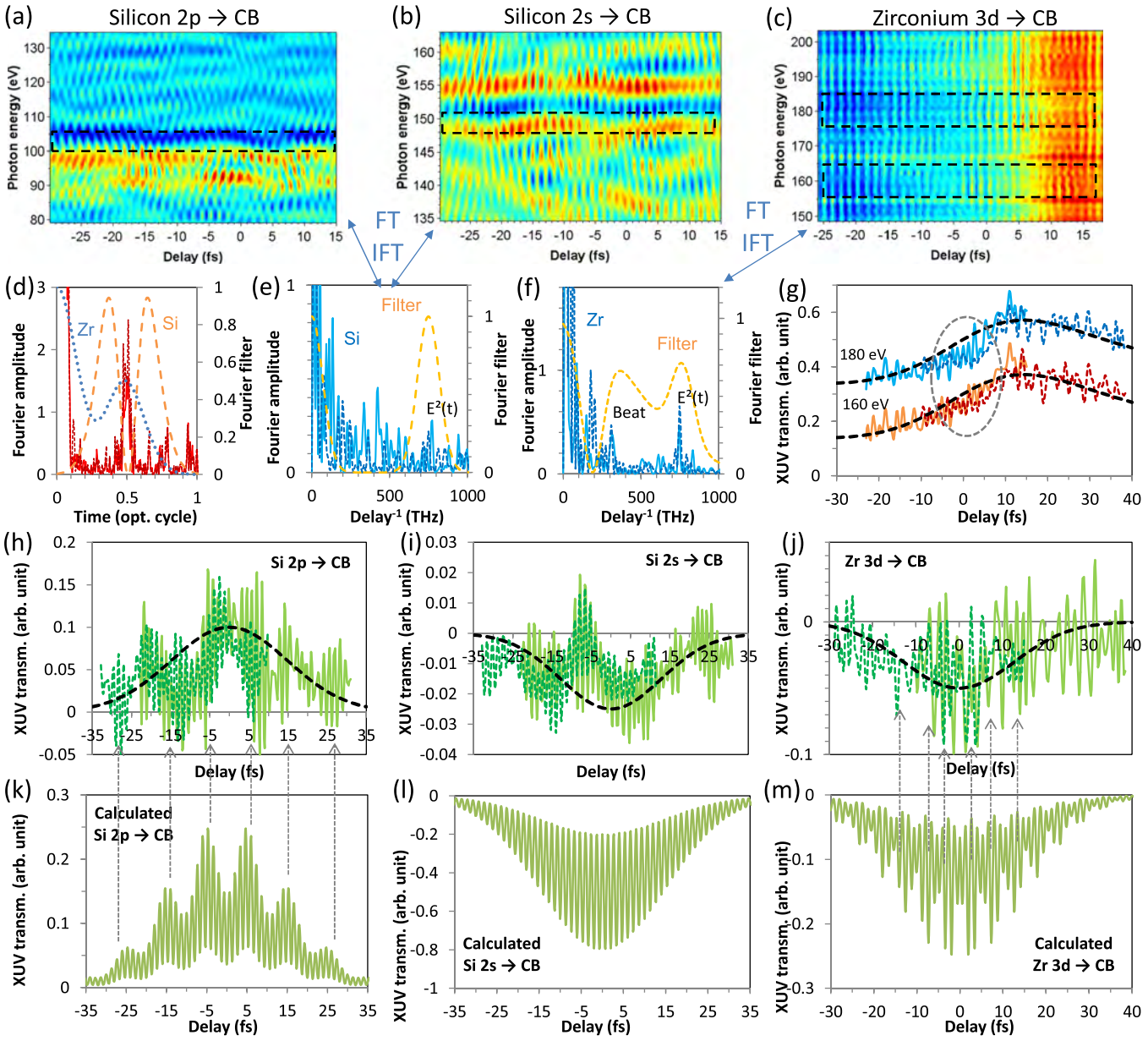

FIG. 6. The XUV transmission spectra around (a) Si $L_{2,3}$, (b) Si L_1, and (c) Zr $M_{4,5}$ edges were measured with attosecond temporal resolution. (d)–(f) The 2D Fourier transforms of the measured data sets were used to identify the involving processes, and suitable Fourier filters were applied to evaluate the measurements and to produce panels (a)–(c). (g)–(m) The evaluated results are plotted together with the theoretical predictions (see details in the text). The normalized color scales in (a) and (b) are the same as in Fig. 4(e) and in (c) as in Fig. 4(a).

the measurements can be recognized, which is similar on both subsequent measurement series. The background of this structure is, however, not clear; it may come from deviations from the Gaussian shape of the laser pulse, from the temporal shape of the generated harmonic pulses, or from some fast electron excitation and relaxation within the CB.

IV. DISCUSSIONS AND CONCLUSIONS

We examined the laser-dressing effects of the NIR pulses of a Ti:sapphire laser system on the wave function of the CB of thin Si and Zr films with core-level attosecond time-resolved XUV spectroscopy. The wave function was probed by high harmonic pulses from a source generating XUV spectra in the 70–230 eV spectral range via exciting core-level electrons into the conduction and observing the change of the XUV transmission. Three transitions were used, namely the $2p \rightarrow$ CB and the $2s \rightarrow$ CB transitions of Si and the $3d \rightarrow$ CB transition of Zr at near 100 eV, 150 eV, and 180 eV, respectively. We observed a slow change in transmission by the envelope and a fast change by the electric field carrier of the dressing laser pulse. The developed theory predicted an increase of the transmission at the $2p \rightarrow$ CB transition and a decrease at the $2s \rightarrow$ CB and $3d \rightarrow$ CB transitions, which were fully observed in the experiments. The theory recognized this difference as the consequence of the symmetry of the CS

wave functions and the symmetry change of the CB wave function via the electric field of the laser pulse.

The measurements in all cases demanded a high temporal resolution to deduce real events from undesirable ones. We made the measurements with both 2 fs and 200 as temporal steps to follow slower and faster processes. The electric field of the laser pulse caused precise controlled alterations of the electrons in the CB and another attosecond pulse train in the XUV spectral range imaged a colored shadow diagram of this alterations. The applied Fourier evaluation technique with miscellaneous chromatic filters served to distinguish and engrave the individually occurred excitation-relaxation processes mixed in these projected pictures.

Beyond the fast oscillation in the XUV transmission caused by the electric field of the laser having a period of 1.3 fs , quantum beats from the $2p_{1/2}$ and $2p_{3/2}$ levels of Si with a period of 20.7 fs and beats from the $3d_{3/2}$ and $3d_{5/2}$ levels of Zr with a period of 3.6 fs were recognized. Furthermore, the effect of the band-to-band electron excitation in Zr and different long and short period phonon modes were found in both Si and Zr.

Our paper recognized ultrafast electronic processes in the CB of semiconductors and metals and provided theoretical support to help the development of even faster electronics for high-speed optical detectors and optical communications.

ACKNOWLEDGMENTS

This paper was supported by the EC's 7th Framework Program (Grant No. 284464, Laserlab Europe HIJ-FSU0019152 and HIJ-FSU001975), the ERC Starting Grant No. 258603 and the EU-FET-Open 664732 "nuClock," the Spanish Ministry of Economy and Competitiveness through "Plan Nacional" (FIS2014-51997-R), and the Japanese Society for the Promotion of Science "KAKENHI 26286078."

APPENDIX

The transient XUV absorption of laser-dressed solids is modeled as follows: The electric field of the NIR laser pulse alters the wave function of the unoccupied level of the CB and consequently alters the absorption of the XUV radiation. We consider no change of the core-level wave functions because of the shielding effect of the outer electron shells. The so-called "dressing" laser field might excite electrons from the VB to the CB or within the CB, but in the present paper, we are not interested in these band-to-band transitions. Here we concentrate only on the core-to-band transitions and the dressing effect of the electric field of the illuminating laser pulse.

Considering dipole transitions, the transition probability between two quantum states of energies E_j and E_m when the system is illuminated with a resonant laser field of frequency ω, such that $\hbar\omega = E_m - E_j$, is given by Fermi's golden rule [36], from which the absorption cross section can be easily derived:

$$\sigma_a = \frac{2\pi e^2}{\hbar c \varepsilon_0} \rho_m \Delta E_m |\langle \Psi_m | x | \Psi_j \rangle|^2. \tag{A1}$$

In Eq. (A1), $\rho_m \Delta E_m$ gives the number of states within the examined energy range ΔE_m, with ρ_m being the density of state (DOS) of the final state (m = CB or VB). The DOS of Si and Zr can be found in several publications, e.g., Refs. [34,35,38].

To calculate the absorption cross section in Eq. (A1) and the effect of the NIR laser field, the wave functions of the core and band states are obtained as follows. (i) We assume that a weak XUV probe pulse moves one electron from a localized atomic CS (Fig. 3, blue thick solid lines) into a delocalized state of the CB (gray thick solid line in Fig. 3) and leaves the VB unaffected. To calculate the quantum states and the wave functions in the CB, we consider the single active electron approximation together with an effective periodic potential, which is formed by the ionic cores and the electrons of the VB. The electron in the CB feels only the effect of this periodic potential. (ii) We use the lattice vector expansion [39] and define the periodic potential as a Fourier series with the reciprocal lattice constant $G = 2\pi/a$:

$$U(x) = \sum_m U_m e^{i(mGx + 2\alpha_m)} = U(x + a), \tag{A2}$$

where a is the lattice constant, i.e., the distance between the atoms in the one dimensional lattice. The U_m is the amplitude of the mth Fourier component, with $U_{-m} = U_m$ and $\alpha_0 = 0$. The U_0 is negative and represents a potential energy below the continuum level for bounded electrons. A periodic potential is drawn in Fig. 3 (gray thin solid line), where we assume $U_m \sim 1/m^2$. The external laser field F_l polarizes the atoms in the lattice by displacing the bounded electrons in the VB, which modifies the shape of the periodic potential. The effect of F_l is treated as a linear perturbation (quasistatic approximation) by the phases α_m in Eq. (A2),

$$\alpha_m = \chi_m F_l, \tag{A3}$$

so that without the external field, $\alpha_m = 0$. An example of the effect of the laser field on the periodic potential is shown in Fig. 3 (red thin dotted line).

In order to describe the laser-dressed states in the solid, we hence solve the one-dimensional Schrödinger equation using the periodic potential given by Eqs. (A2) and (A3). For simplicity, we consider only the first order terms $m = 0, \pm 1$, which gives

$$U(x) = U_0 + 2U_1 \cos(Gx + 2\alpha_1). \tag{A4}$$

Using Bloch's theorem, near the band gap ($k \approx 0$), two plane-wave solutions can be obtained:

$$\Psi_\pm(x) = \frac{1}{\sqrt{2a}} [e^{+i(Gx+2\alpha_1)/2} \pm e^{-i(Gx+2\alpha_1)/2}], \tag{A5}$$

which give the normalized wave functions of the VBs and CBs as

$$\Psi_{\mathrm{CB}}(x) = \Psi_+(x) = \sqrt{\frac{2}{a}} \cos\left(\frac{1}{2}Gx + \alpha_1\right), \tag{A6}$$

$$\Psi_{\mathrm{VB}}(x) = \Psi_-(x) = i\sqrt{\frac{2}{a}} \sin\left(\frac{1}{2}Gx + \alpha_1\right), \tag{A7}$$

with energies

$$E_{\pm}(k) = \frac{\hbar^2 k^2}{2m} \pm \sqrt{\frac{\hbar^2 k^2}{2m}\frac{\hbar^2 G^2}{2m} + U_1^2}. \tag{A8}$$

The two energies $E_{\pm}(k)$ in Eq. (A8) therefore give the splitting between the two energy dispersion functions $[E(k)]$ of the Ψ_{CB} and Ψ_{VB} states, respectively. The minimal band gap is defined as $\Delta E_g = 2|U_1|$ at $k = 0$. Following the convention in XAS, we measure every energy level relative to the Fermi level $E_F = 0$, which provides $U_0 = -\hbar^2 G^2/8m$ at $k = 0$. Therefore, in the case of a material with known energy band gap and lattice constant, the potential described in Eq. (A4) is known.

Usually, the transitions are considered between two Bloch states of the electron, namely between the VB and the CB states. Here, however, we consider transitions between a CS of an electron (localized and bounded to an atom) and a Bloch state in the VB or in the CB, considering the wave functions given by Eqs. (A6) and (A7). The wave function of the CS is approximated by a hydrogenlike radial wave function. In the experiments, we measured how the XUV transmission spectra changed in time due to the effect of the illuminating laser field; therefore, the calculation of the absolute value of the transition probability is not necessary. Indeed, what affects the transition probability is the symmetry of the core wave function, namely whether it is symmetric, antisymmetric, or asymmetric. As seen in Eqs. (A6) and (A7), the wave functions Ψ_{CB} and Ψ_{VB} are symmetric and antisymmetric, respectively. Selection rules from the dipole approximation forbid symmetric-to-symmetric and antisymmetric-to-antisymmetric transitions. If the external electric field of the laser modifies the symmetry of the CB or VB wave functions (as shown in Fig. 3 with a red dashed line), the probability of the transitions changes such that they can become possible or forbidden. Therefore, the usage of the hydrogenlike radial wave functions with the suitable symmetry fulfills the requirements in our analysis.

We examine the transition from the $2p$ (L_2 and L_3 edges) and $2s$ (L_1 edge) CSs of Si and the transition from the $3d$ (M_4 and M_5 edges) CS of Zr at 100 eV, 150 eV, and 180 eV photon energies, respectively. While the wave function of the $2p$ state is antisymmetric, that of the $2s$ and $3d$ states is symmetric. The corresponding normalized wave functions are

$$\begin{aligned} \Psi_{2s} &= 2\sqrt{\gamma_{2s}}(1-\gamma_{2s}|x|)e^{-\gamma_{2s}|x|}, \\ \Psi_{2p} &= 2\sqrt{\gamma_{2p}^3}\,x e^{-\gamma_{2p}|x|}, \\ \text{and}\quad \Psi_{3d} &= 4\sqrt{\gamma_{3d}^5}\,x^2 e^{-\gamma_{3d}|x|}. \end{aligned} \tag{A9}$$

The effective charge of the core can be obtained from the energy of the orbital with principal quantum number n as $E_n = -13.6\,\text{eV}\frac{Z_{\text{eff}}^2}{n^2}$, and the reciprocal orbital radius γ is given by the formula $\gamma^{-1} = \frac{na_B}{Z_{\text{eff}}}$, where $a_B = 52.9\,\text{pm}$ is the Bohr radius. For Si, $E_{2p} = -99.6\,\text{eV}$ and $E_{2s} = -149.7\,\text{eV}$; for Zr, $E_{3d} = -180\,\text{eV}$, which gives $Z_{2p,\text{eff}} = 5.4$, $Z_{2s,\text{eff}} = 6.6$, and $Z_{3d,\text{eff}} = 10.9$, respectively, with $\gamma_{2p}^{-1} = 19.6\,\text{pm}$, $\gamma_{2s}^{-1} = 15.9\,\text{pm}$, and $\gamma_{3d}^{-1} = 14.6\,\text{pm}$. The lattice constants for Si and Zr are 543 pm and 323(515) pm, respectively. Therefore, all wave functions and parameters are known to calculate the transition probabilities and absorption cross sections.

The cross section in Eq. (A1) can be obtained by calculating the dipole matrix elements $d_{j,\pm} = \langle \Psi_{\pm}|x|\Psi_j\rangle$, with $j = 2p, 2s$, or $3d$. Since the electron orbitals of the core electrons are almost two orders of magnitude smaller than the lattice constant, we assume $\gamma \gg G$. The absorption cross-sections of the different transitions are thus readily derived by using the delocalized wave functions in the form of Eqs. (A6) and (A7) and the core wave functions in the form of Eq. (A9). Using the notation $j = 2p, 2s$, or $3d$ and $m =$ CB or VB, for the transitions $2p \to$ CB, $2s \to$ VB, $3d \to$ VB, we have

$$\sigma_{j,m} \approx A_{j,m}\cos^2\alpha_1, \tag{A10}$$

and for the transitions $2p \to$ VB, $2s \to$ CB, and $3d \to$ CB,

$$\sigma_{j,m} \approx A_{j,m}\sin^2\alpha_1, \tag{A11}$$

where $A_{2p,m} = \frac{2^6\pi e^2\rho_m\Delta E_m}{\hbar c\varepsilon_0(a\gamma_{2p})^3}a^2$, $A_{2s,m} = \frac{2^8\pi^3 e^2\rho_m\Delta E_m}{\hbar c\varepsilon_0(a\gamma_{2s})^5}a^2$, and $A_{3d,m} = \frac{2^{14}\pi^3 e^2\rho_m\Delta E_m}{\hbar c\varepsilon_0(a\gamma_{3d})^5}a^2$.

We assume a suitably weak laser field, which polarizes the material and perturbs the periodic potential weakly. This means that the change of the potential can be described with a small parameter α_1 [see Eq. (A3)], and it can hence be considered as a small perturbation, with $\cos^2\alpha_1 \approx 1 - \alpha_1^2$ and $\sin^2\alpha_1 \approx \alpha_1^2$. Using Eq. (A3), we have

$$\begin{aligned} \alpha_1 &= \chi_1 F(\tau) = \chi_1 F_0(\tau)\sin(\omega_0\tau), \\ \text{or}\quad \alpha_1^2 &= \chi_1^2 I(\tau) = \chi_1^2 I_0(\tau)\sin^2(\omega_0\tau), \end{aligned} \tag{A12}$$

where ω_0 is the angular frequency of the laser, $F(\tau)$ is the strength of the electric field, and $I(\tau)$ is the intensity envelope of the laser pulse at the time that the XUV pulse arrives, so τ can be considered as the delay between the XUV pulse and the laser field. Substituting Eq. (A12) into Eq. (A10) and (A11), we obtain

$$\Delta\sigma_{j,m} \approx \mp\frac{\chi_1^2 A_{j,m}}{c\varepsilon_0} I_0(\tau)\sin^2(\omega_0\tau), \tag{A13}$$

and from Eq. (1) the transmission change is

$$\Delta T_{j,m} \approx \pm T_{j,m} I_0(\tau)\sin^2(\omega_0\tau), \tag{A14}$$

where $T_{j,m} = A_{j,m}\frac{\chi_1^2}{c\varepsilon_0}T_0 n_a d$, where $j = 2p, 2s$, or $3d$ and $m =$ CB or VB. In Eq. (A14), the sign $(+)$ corresponds to the $2p \to$ CB, $2s \to$ VB, and $3d \to$ VB transitions, while the sign $(-)$ is for the $2p \to$ VB, $2s \to$ CB, and $3d \to$ CB transitions.

From Eq. (A14), we can thus make predictions of what one can see in the experiments. On the one hand, without the dressing laser field ($\alpha_1 = 0$), Eq. (A10) predicts a strong absorption (small transmission) at the $2p \to$ CB transition ($\sim$100 eV, Si). This means that the CB is situated just above the $L_{2,3}$ edge of Si within a few eV DOS spectral range. [37] With the dressing NIR laser field, Eq. (A14) predicts that the transmission depends on the delay τ between the XUV pulse and the laser electric field. It predicts a slow increase of the XUV transmission due to the envelope of the laser pulse $I(\tau)$ together with a very fast oscillation $[\sin^2(\omega_0\tau)]$ of transmission at half optical period of the laser pulse ($\sim$1.34 fs). On the other hand, Eqs. (A11) and (A14) predict exactly the opposite for the $2s \to$ CB transition of Si at 150 eV and the $3d \to$ CB transition of Zr at 180 eV. At these absorption edges,

the originally large transmission of XUV has to decrease due to the dressing laser field, caused by a combination between the slow change of the pulse envelope and the fast oscillation of the squared electric field carrier with half optical period.

A. Beat between transitions

In Eq. (2), only one possible transition is considered at a certain XUV wavelength. This is the correct case for the $2s \rightarrow$ CB transition of Si at 150 eV. However, for the $2p \rightarrow$ CB and $3d \rightarrow$ CB transitions of Si and Zr (see Fig. 2), respectively, there are two near-lying levels and consequently two possible transitions in each case. The two levels are $2p_{1/2}$ and $2p_{3/2}$ at 99.82 eV and 99.42 eV for Si and $3d_{3/2}$ and $3d_{5/2}$ at 181.1 eV and 178.8 eV for Zr. The distances of 0.4 eV and 2.3 eV between the levels are smaller than the width of the CB so that for a certain XUV wavelength, both transitions are possible. To understand how this appears in the measurement, the time dependent dipole matrix element is written as

$$d(t) = eF_{\mathrm{XUV},0}e^{i\omega_{\mathrm{XUV}}t}\langle\Psi_{b1}e^{iE_{b1}/\hbar t} + \Psi_{b2}e^{iE_{b2}/\hbar t}| \times x|\Psi_{c1}e^{iE_{c1}/\hbar t} + \Psi_{c2}e^{iE_{c2}/\hbar t}\rangle, \tag{A15}$$

where Ψ_{b1}, Ψ_{b2} are the wave functions of the two band states with energies E_{b1} and E_{b2}, and Ψ_{c1}, Ψ_{c2} are the wave functions of the two CSs with energies E_{c1} and E_{c2}. The XUV field is resonant with the two transitions, which means that $\hbar\omega_{\mathrm{XUV}} = E_{b1} - E_{c1} = E_{b2} - E_{c2}$. Equation (A15) can be separated into four terms using the notation $\Delta E = E_{b1} - E_{b2} = E_{c1} - E_{c2}$ as

$$\begin{aligned} d(t) = {} & eF_{\mathrm{XUV},0}\langle\Psi_{b1}|x|\Psi_{c1}\rangle + eF_{\mathrm{XUV},0}\langle\Psi_{b2}|x|\Psi_{c2}\rangle \\ & + eF_{\mathrm{XUV},0}e^{-i\Delta E/\hbar t}\langle\Psi_{b1}|x|\Psi_{c2}\rangle \\ & + eF_{\mathrm{XUV},0}e^{i\Delta E/\hbar t}\langle\Psi_{b2}|x|\Psi_{c1}\rangle. \end{aligned} \tag{A16}$$

Because the two levels lie close to each other, their wave functions hardly differ; therefore, we assume $\Psi_{b1} \approx \Psi_{b2} = \Psi_b$ and $\Psi_{c1} \approx \Psi_{c2} = \Psi_c$, with which Eq. (A16) takes the simple form

$$d(t) = 4eF_{\mathrm{XUV},0}\langle\Psi_b|x|\Psi_c\rangle\cos^2\left(\frac{\Delta E}{2\hbar}t\right). \tag{A17}$$

This results in the appearance of a beat signal in the XUV transmission in Eq. (A14) with angular frequency of $\Omega = \Delta E/2\hbar$:

$$\Delta T_{j,m} \approx \pm T_{j,m} I_0(\tau)\sin^2(\omega_0\tau)\cos^4(\Omega\tau), \tag{A18}$$

where the sign (+) is for $2p \rightarrow$ CB transition and the sign (−) is for $3d \rightarrow$ CB. In the case of Si, the energy difference between the $2p_{1/2}$ and $2p_{3/2}$ levels is 0.4 eV, which means a beat of frequency 48.4 THz or period of 20.7 fs. For the $3d_{3/2}$ and $3d_{5/2}$ levels of Zr, this gives 2.3 eV, 278.0 THz, and 3.6 fs.

[1] O. Kwon and D. Kim, Appl. Phys. Lett. **108**, 191112 (2016).
[2] K.-J. Boller, A. Imamoglu, and S. E. Harris, Phys. Rev. Lett. **66**, 2593 (1991).
[3] Z.-H. Loh and S. R. Leone, J. Phys. Chem. Lett. **4**, 292 (2013).
[4] M. Wu, S. Chen, S. Camp, K. J. Schafer, and M. B. Gaarde, J. Phys. B. **49**, 062003 (2016).
[5] W. Cao, E. R. Warrick, D. M. Neumark, and S. R. Leone, New J. Phys. **18**, 013041 (2016).
[6] X. Wang, M. Chini, Y. Cheng, Y. Wu, X.-M. Tong, and Z. Chang, Phys. Rev. A **87**, 063413 (2013).
[7] M. Reduzzi, J. Hummert, A. Dubrouil, F. Calegari, M. Nisoli, F. Frassetto, L. Poletto, S. Chen, M. Wu, M. B. Gaarde, K. Schafer, and G. Sansone, Phys. Rev. A **92**, 033408 (2015).
[8] C. Ott, A. Kaldun, L. Argenti, P. Raith, K. Meyer, M. Laux, Y. Zhang, A. Blattermann, S. Hagstotz, T. Ding, R. Heck, J. Madronero, F. Martin, and T. Pfeifer, Nature **516**, 374 (2014).
[9] A. Trabattoni, M. Klinker, J. González-Vázquez, C. Liu, G. Sansone, R. Linguerri, M. Hochlaf, J. Klei, M. J. J. Vrakking, F. Martín, M. Nisoli, and F. Calegari, Phys. Rev. X **5**, 041053 (2015).
[10] E. R. Hosler and S. R. Leone, Phys. Rev. A **88**, 023420 (2013).
[11] A. Marciniak, V. Despre, T. Barillot, A. Rouzee, M. C. E. Galbraith, J. Klei, C.-H. Yang, C. T. L. Smeenk, V. Loriot, S. N. Reddy, A. G. G. M. Tielens, S. Mahapatra, A. I. Kuleff, M. J. J. Vrakking, and F. Lepine, Nature Commun. **6**, 7909 (2015).
[12] E. Goulielmakis, Z.-H. Loh, A. Wirth, R. Santra, N. Rohringer, V. S. Yakovlev, S. Zherebtsov, T. Pfeifer, A. M. Azzeer, M. F. Kling, S. R. Leone, and F. Krausz, Nature **466**, 739 (2010).
[13] A. N. Pfeiffer and S. R. Leone, Phys. Rev. A **85**, 053422 (2012).
[14] M.-F. Lin, A. N. Pfeiffer, D. M. Neumark, S. R. Leone, and O. Gessner, J. Chem. Phys. **137**, 244305 (2012).
[15] M. Chini, B. Zhao, H. Wang, Y. Cheng, S. X. Hu, and Z. Chang, Phys. Rev. Lett. **109**, 073601 (2012).
[16] M. Fushitani, C.-N. Liu, A. Matsuda, T. Endo, Y. Toida, M. Nagasono, T. Togashi, M. Yabashi, T. Ishikawa, Y. Hikosaka, T. Morishita, and A. Hishikawa, Nature Photon. **10**, 102 (2015).
[17] A. R. Beck, B. Bernhardt, E. R. Warrick, M. Wu, S. Chen, M. B. Gaarde, K. J. Schafer, D. M. Neumark, and S. R. Leone, New J. Phys. **16**, 113016 (2014).
[18] N. Shivaram, X.-M. Tong, H. Timmers, and A. Sandhu, J. Phys. B **49**, 055601 (2016).
[19] K. Murakami, H. C. Gerritsen, H. van Brug, F. Bijkerk, F. W. Saris, and M. J. van der Wiel, Phys. Rev. Lett. **56**, 655 (1986).
[20] H. Nakano, Y. Goto, P. Lu, T. Nishikawa, and N. Uesugi, Appl. Phys. Lett. **75**, 2350 (1999).
[21] E. Seres and C. Spielmann, Appl. Phys. Lett. **91**, 121919 (2007).
[22] E. Seres and C. Spielmann, J. Mod. Optics **55**, 2643 (2008).
[23] E. Seres, J. Seres, and C. Spielmann, Appl. Phys. A **96**, 43 (2009).
[24] E. Seres and C. Spielmann, *Femtosecond-Scale Optics*, edited by Anatoli V. Andreev, *InTech*, 203 (2011).
[25] M. Schultze, E. M. Bothschafter, A. Sommer, S. Holzner, W. Schweinberger, M. Fiess, M. Hofstetter, R. Kienberger, V. Apalkov, V. S. Yakovlev, M. I. Stockman, and F. Krausz, Nature **493**, 75 (2013).
[26] M. Schultze, K. Ramasesha, C. D. Pemmaraju, S. A. Sato, D. Whitmore, A. Gandman, J. S. Prell, L. J. Borja, D. Prendergast, K. Yabana, D. M. Neumark, and S. R. Leone, Science **346**, 1348 (2014).
[27] H. Mashiko, K. Oguri, T. Yamaguchi, A. Suda, and H. Gotoh, Nat. Pnys. **12**, 741 (2016).

[28] C.-M. Jiang, L. R. Baker, J. M. Lucas, J. Vura-Weis, A. P. Alivisatos, and S. R. Leone, J. Phys. Chem. C **118**, 22774 (2014).

[29] J. Seres, E. Seres, B. Landgraf, B. Ecker, B. Aurand, A. Hoffmann, G. Winkler, S. Namba, T. Kuehl, and C. Spielmann, Sci. Rep. **4**, 4254 (2014).

[30] C. Serrat, D. Roca, J. M. Budesca, J. Seres, E. Seres, B. Aurand, A. Hoffmann, S. Namba, T. Kuehl, and C. Spielmann, Opt. Express **24**, 8028 (2016).

[31] F. C. Brown, R. Z. Bachrach, and M. Skibowski, Phys. Rev. B **15**, 4781 (1977).

[32] B. L. Henke, E. M. Gullikson, and J. C. Davis, At. Data Nucl. Data Tables **54**, 181 (1993).

[33] M. D. Kluge and J. R. Ray, Phys. Rev. B **37**, 4132 (1988).

[34] M. Lindgren and I. Panas, RSC Adv. **4**, 11050 (2014).

[35] J. Cai, Y. S. Raptis, and E. Anastassakis, Appl. Phys. Lett. **62**, 2781 (1993).

[36] Y. M. Galperin, Introduction to Modern Solid State Physics, chapter 9.3, pages 190–191, Fermi's golden rule with dipole approximation. **9**

[37] J. D. Joannopoulos and M. L. Cohen, Phys. Rev. B **7**, 2644 (1973).

[38] Z.-W. Lu, D. Singh, and H. Krakauer, Phys. Rev. B **36**, 7335 (1987).

[39] M. Grundmann, *The Physics of Semiconductors*, Chapter 6 (Springer-Verlag, Berlin, 2006).